Rotary DNA Motors

Charles Doering,* Bard Ermentrout,‡ and George Oster§

*Center for Nonlinear Studies, Los Alamos National Laboratory, Los Alamos, New Mexico 87545; ‡Department of Mathematics, University of Pittsburgh, Pittsburgh, Pennsylvania 15260; and §Department of Molecular and Cellular Biology, University of California, Berkeley, California 94720-3112 USA

ABSTRACT Many molecular motors move unidirectionally along a DNA strand powered by nucleotide hydrolysis. These motors are multimeric ATPases with more than one hydrolysis site. We present here a model for how these motors generate the requisite force to process along their DNA track. This novel mechanism for force generation is based on a fluctuating electrostatic field driven by nucleotide hydrolysis. We apply the principle to explain the motion of certain DNA helicases and the portal protein, the motor that bacteriophages use to pump the genome into their capsids. The motor can reverse its direction without reversing the polarity of its electrostatic field, that is, without major structural modifications of the protein. We also show that the motor can be driven by an ion gradient; thus the mechanism may apply as well to the bacterial flagellar motor and to ATP synthase.

INTRODUCTION

A variety of protein motors have the property that they process unidirectionally along a polymer track, driven by nucleotide hydrolysis. Actin and tubulin provide the tracks for the most well-studied examples, myosin, kinesin, and dynein. DNA is also traversed by a medley of protein motors that replicate, repair, and package the genome. These protein machines differ from myosin and kinesin in several ways that suggest their mechanical mechanism is different. First, certain DNA motors appear to be rotary, rather than reciprocating; i.e., they process not by "walking" along their track, but by rotating about it, so that their procession is helical rather than linear. Moreover, they are multimeric and may hydrolyze nucleotides at several catalytic sites (Patel and Hingorani, 1994; Patel et al., 1994). Although it is clear that these motors are driven by nucleotide hydrolysis, the precise mechanism by which phosphate bond energy is transduced into a directed force remains mysterious. Here we propose a novel mechanism for rotary molecular motors that we apply to a model for the portal protein and certain DNA helicases.

For many bacteriophages, the culmination of assembly involves the insertion of several hundred kilobases of genomic DNA into the capsid head. This is an astounding packaging job, for the length of the DNA is ~3500 times as long as the capsid, yet the entire process is completed within 15–90 s, which suggests a velocity of more than 1 μm/s. Although the packaging mechanism remains largely mysterious, several known features provide some clues. First, one ATP is hydrolyzed in the packaging of two base pairs, or 9×10^3 ATPs are needed to package

the 1.8×10^4 base pairs in the phage $\phi 29$ (Guo et al., 1987). This suggests that DNA is driven into the capsid by some sort of ATPase motor. Second, DNA is inserted through a protein complex at the capsid base, the portal protein, or "connector" (Black, 1988; Earnshaw and Casjens, 1980; Valpuesta and Carrascosa, 1994). The molecular geometry of this structure is known for several phage species (Carazo et al., 1986; Casjens et al., 1992; Donate and Carrascosa, 1991; Dube et al., 1993; Valpuesta et al., 1992), and its geometry and symmetries suggest that DNA may be inserted in a rotary and/or translational motion through the central channel.

DNA helicases are also nucleotide-driven motors that can translocate along double- or single-stranded DNA at speeds of up to 1000 nucleotides/s ~ 34 nm/s. Although rolling or walking mechanisms have been suggested for certain helicases (Lohman, 1992; Wong and Lohman, 1992), the structure of some helicases is similar to, but simpler than, that of the portal proteins, suggesting a rotary motion. For example, the T7 gene4 helicase is a doughnut-shaped hexameric ATPase with three hydrolysis sites that translocates along ss-DNA (Egelman et al., 1995; Hingorani and Patel, 1993; Patel and Hingorani, 1994; Patel et al., 1994). Fig. 1 shows the geometry of a portal protein from T3 bacteriophage and the helicase from T7 bacteriophage.

Here we shall present a model for the mechanochemistry of these two DNA motors, which we propose operate by similar mechanisms. For simplicity, we shall focus on the T7 helicase.

THE FLASHING FIELD MODEL

The model is based on the following central assumption (see Fig. 1): *Binding of ATP to a hydrolysis site induces a conformational change that exposes a pair of negative and positive charge regions near the inner surface of the channel.*

FIGURE 1 Geometry of the helicase and portal proteins, showing their tubular, multimeric structure. (*Top*) Schematic of the portal protein of the bacteriophage T3 showing the DNA threading through the portal orifice. (*Bottom*) Schematic cross-sectional view of the T7 helicase showing a ss-DNA strand threading through the hole. (*Bottom right*) Top view showing the six subunits assembled into a ring with a 2.5–3-nm hole. We have shown the ATP binding sites located at the junctions between subunits, although their exact location is not clear. As required by the model, the nucleotide binding sites are contiguous to the charge-pair sites just beneath the surface of the hole. In both proteins, the 8–12-nm length of the hole accommodates about 1½-2 turns of the DNA helix. On this length scale ds-DNA is quite stiff.
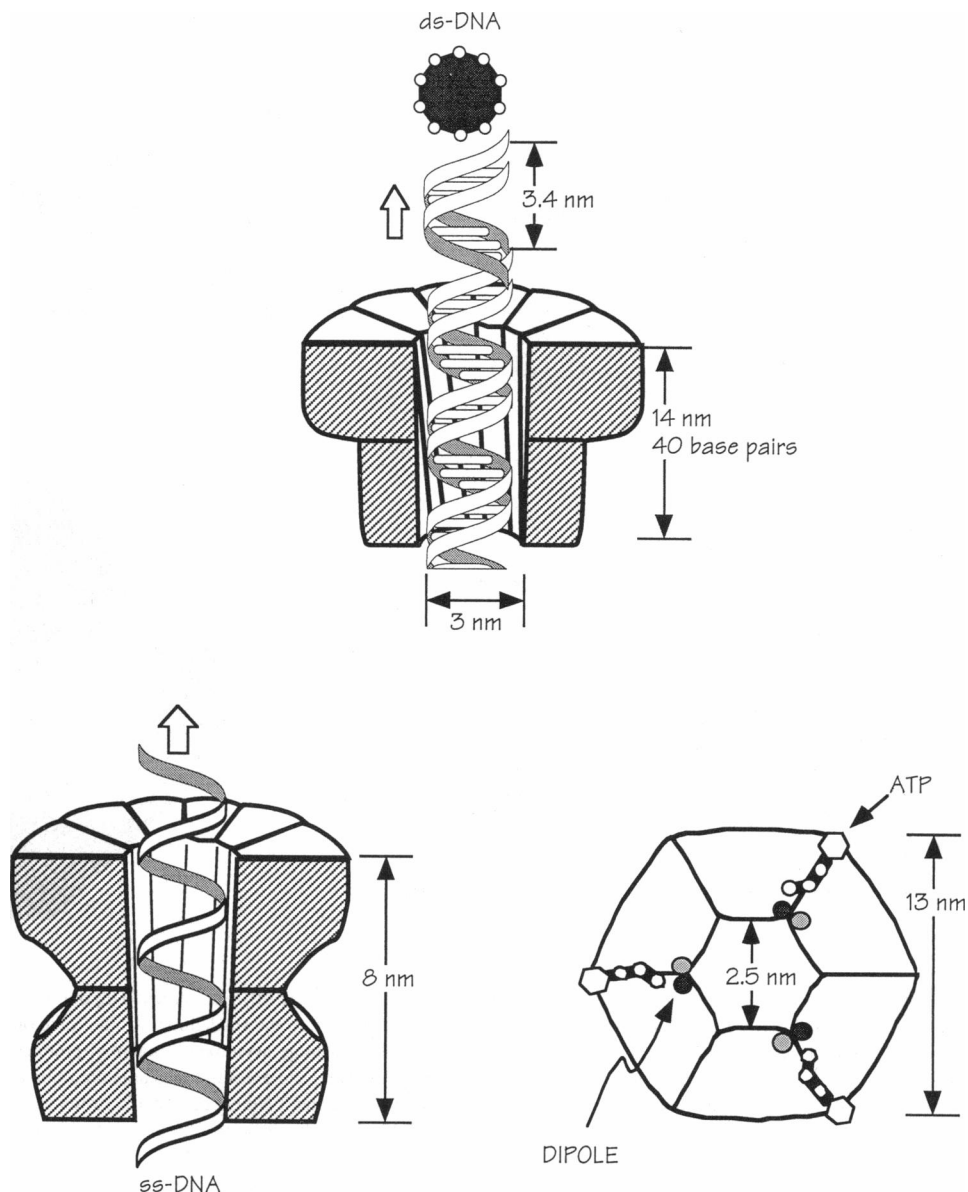
The charged regions are not of equal size, and they are oriented at an angle to the circumferential meridian. We will assume that there is one charge pair region per nucleotide hydrolysis site, and that the axes of the charge pair regions are tilted with respect to the axis of the hole. The helicase binds three nucleotides at a time, and so we infer it has three hydrolysis sites (Patel et al., 1994; Patel and Hingorani, 1995); however, the portal protein has perhaps 12 or 13 hydrolysis sites, located in two tiers (Casjens et al., 1992; Dube et al., 1993). As we will see, the pattern of hydrolysis affects the performance of the motor (analogous to the firing sequence of a car engine). Therefore, if each hydrolysis site controls the expression of a single charge pair then, for more than a few hydrolysis sites, the number of firing sequences becomes too large to compute.

Qualitatively, the model works like this. The negatively charged phosphates spaced along the backbone of the DNA strand interact sequentially with the field of the charge pair regions as they "flash" on and off with the binding and hydrolysis of ATP. Each charge pair field gives the closest phosphate(s) an "electrostatic push" in the direction of the charge pair axis. The net effect of the charge pairs flashing on and off creates a sustained torsional and axial thrust. It turns out that the order in which the fields flash is not too important; even random flashing will drive the rotation. Note that the motor is an electrostatic machine that transduces strain fluctuations generated by nucleotide hydrolysis into a fluctuating electric field. Biased diffusion plays no role in torque generation; Brownian motion serves only as a "lubricant" to ensure the rotor does not hang up in local energy minima. Fig. 2 illustrates the model geometry and the operating principle.

APPROXIMATIONS AND PARAMETER VALUES

In deriving the model equations we make several simplifying approximations. None of these are essential to the mech-
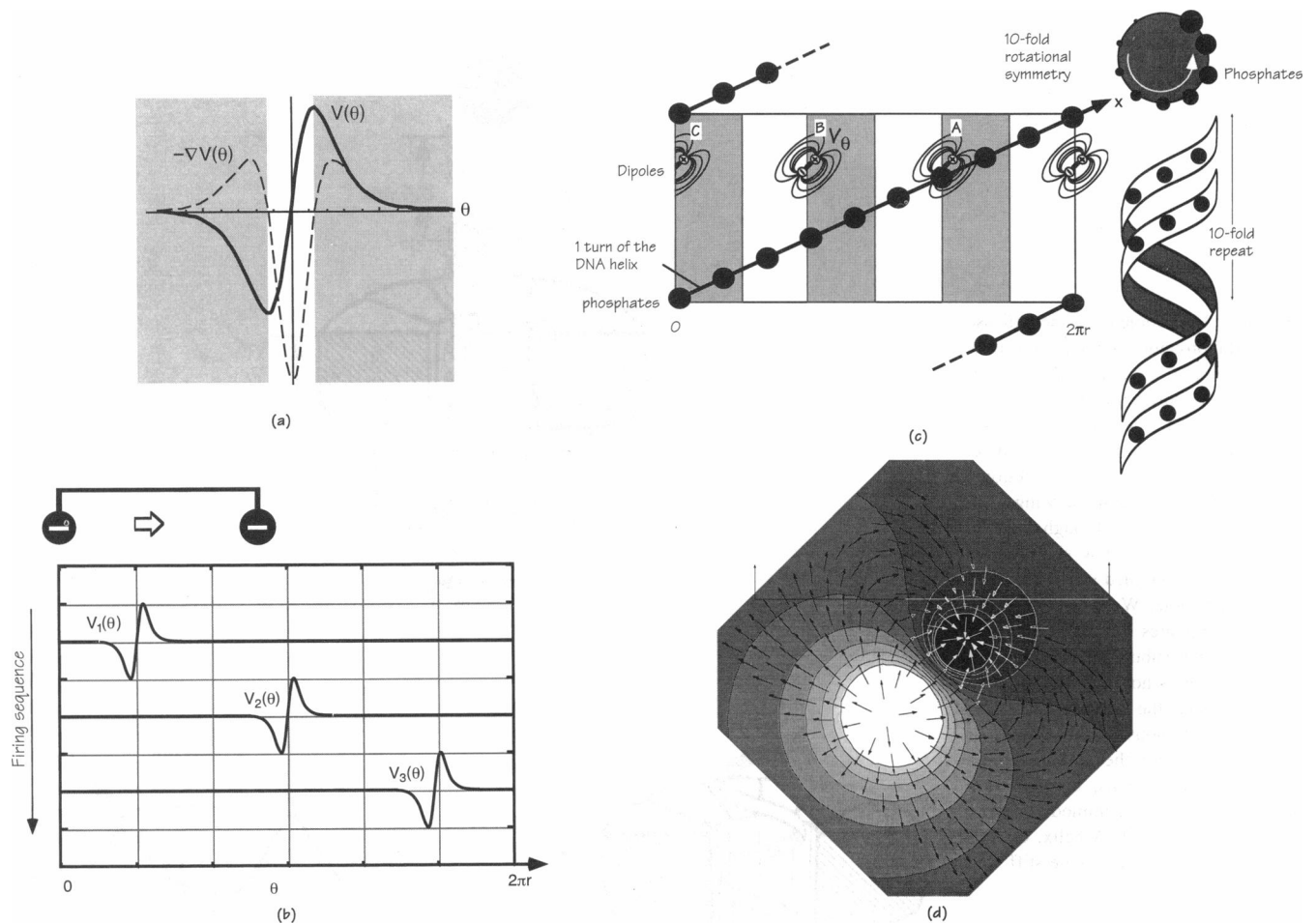
FIGURE 2　(a) The potential (*solid line*) and the force (*dashed line*) of a single off-axis, screened dipole (Eq. 2) seen by a single negative phosphate charge along the DNA backbone. The dashed line is the force on a negative charge. In the shaded regions the force on the phosphate is to the right. Although there is a small region (*white*) where the force acts strongly to the left, the flashing, asymmetric potential produces a net force to the right. (b) Illustrating the flashing field principle. A pair of negative charges are rigidly connected and can execute overdamped motion along the x axis under the influence of thermal noise and dipole 1, 2, or 3. The dipoles flash between configurations 1, 2, and 3 either sequentially or randomly, one being "on" at all times. The potentials are each repeated periodically in the x direction. The flashing fields drive the negative charges to the right. (c) The helicase has been slit and unrolled to show the inner surface of the hole. The diagonal line is the phosphate backbone of the DNA; the phosphates are shown as black dots (●). In this figure, the hole contains one turn of the helix. The three dipoles, labeled A, B, and C, are spaced along the top of the hole and inclined with respect to the axis of the hole. Assume that dipole A flashes on; the backbone charge closest to A feels the dipole field and is given both an axial and a circumferential push. This brings another charge into range of dipole B. If dipole B switches on after A switches off, this phosphate is given another push. Thus as the dipoles flash on they exert both an angular and a longitudinal push on the closest phosphates, bringing another phosphate within range of the next dipole's field. Because rotational diffusion is very rapid, "dead spots" do not hang up the DNA motion; i.e., Brownian motion acts as a "lubricant." The unidirectionality is determined by the orientation of the dipole fields. The ability of the motor to reverse its direction of rotation requires an asymmetric field, which we model as a multipole field consisting of a dipole plus an additional positive charge, as shown in d. (d) Potential and field lines for a charge pair tilted at 45°. The positive charge is twice the magnitude of the negative charge. The arrows depict the force experienced by a negative charge in the field. The potential profile in a corresponds to the section shown by the arrows.

anism, but they are necessary to formulating a tractable mathematical model.

　1. The DNA is stiff. This is a good approximation because the persistence length of DNA is about 50 nm, whereas the length of the DNA motors is ≤12 nm.

　2. The DNA strand fits snugly into the hole in the motor. The diameter of a B-DNA strand is ~1.8 nm, whereas the diameter of the hole is 2.5 nm (helicase)–3.7 nm (portal protein); thus there may be considerable wobble accompanying the motion. This greatly increases the complexity of

the computations without adding much to the principle of operation. Therefore, we have simplified the model by neglecting the wobble, e.g., the DNA threads through the hole snugly. In fact, the effective diameter of B-DNA, including hydration and charge, may be larger than that measured diameter, and so the DNA strand may indeed fit snugly into the central passage.

　3. The sizes of the positive and negative charge regions in the charge pairs are unknown, and so for simplicity we have assumed a simple asymmetrical field consisting of a

dipole plus a monopole. (The recently elucidated structure of the F1 portion of ATP synthase shows a triplet of equally spaced, unequal, charged regions lining the orifice facing the γ shaft. Cf. figure 5 of Abrahams et al., 1994.) Because the angle of the field is unknown, we have assumed it is 45°.

4. The dielectric environment of the hole is unknown. Therefore, we have assumed a dielectric constant typical of protein interiors ($\epsilon \sim 4$–7). The central cavity in F1-ATP synthase is hydrophobic (Abrahams et al., 1994), and we have taken this as justification for this assumption.

5. The number of phosphates interacting with each charge pair depends on the fit of the DNA in the motor channel and the interior dielectric environment. We have assumed that only two phosphates sense the electrostatic field at a time. Increasing the number of phosphate charges that sense the field will not alter the qualitative behavior of the model.

6. The net hydrolysis rate is chosen arbitrarily at 100/s. The total flashing rate for ϕ29 portal protein can be obtained from the measured nucleotide hydrolysis rate, ~ 1500 s^{-1}. However, the number of ATPase sites is unknown. For helicase, the net hydrolysis rate has not yet been determined. However, knowing that the velocity is about 1000 nucleotides/s (~ 0.34 μm/s) and assuming completely tight coupling (i.e., one hydrolysis per nucleotide), an upper bound on helicase hydrolysis can be assigned.

Until the detailed structures are known, and the above quantities are available, we can only demonstrate the principle of operation; however, the model points to definite measurable properties.

MODEL EQUATIONS

The equations describing the motion of the motor can be written in two equivalent ways: as stochastic ordinary differential (i.e., Langevin) equations describing the motion of a single motor, or as diffusion (i.e., Fokker-Planck) equations describing the motion of an ensemble of motors (Doering, 1990; Gardiner, 1985; Riskin, 1989). The former are generally easier to understand, simulate numerically, and compare with experiments, whereas the latter are easier to obtain statistical properties of trajectories. We shall present the model as Langevin equations; the equivalent Fokker-Planck equations are presented in the Appendix, along with the computational algorithms we have employed.

The equations describing the motor are as follows. Let θ be the cyclical coordinate of the position of a dipole on the inner surface of the helicase. We put our coordinate system on the DNA, so that it remains stationary while the helicase spins and translates. The circumferential (θ) and translational (z) components of the helicase motion are given by

the pair of Langevin equations:

$$\zeta_\theta \frac{d\theta}{dt} = \underbrace{-\frac{dV(\theta, z, t)}{d\theta}}_{\substack{\text{Torque due} \\ \text{to potentials}}} \underbrace{-\ \tau_\theta}_{\text{Load}} + \underbrace{\sqrt{2\zeta_\theta k_B T} \cdot \xi_\theta(t)}_{\substack{\text{Brownian} \\ \text{motion}}},$$ (1a)

$$0 \le \theta \le 2\pi$$

$$\zeta_z \frac{dz}{dt} = \underbrace{-\frac{dV(\theta, z, t)}{dz}}_{\substack{\text{Axial thrust} \\ \text{due to} \\ \text{potentials}}} \underbrace{-\ \tau_z}_{\text{Load}} + \underbrace{\sqrt{2\zeta_z k_B T} \cdot \xi_z(t)}_{\substack{\text{Brownian} \\ \text{motion}}},$$ (1b)

$$-L \le z \le L.$$

Here the subscripts θ and z refer to rotational and longitudinal quantities, respectively. $\xi_{\theta,z}(t)$ are gaussian white noise processes satisfying $\langle \xi(t) \rangle = 0$, $\langle \xi(t)\ \xi(t - s) \rangle = \delta(t - s)$. The motor is driven by the time variation of the potentials' amplitudes, which are driven by the hydrolysis cycle. Although the magnitudes of the charge regions are not equal, for simplicity we shall begin by modeling the spatial dependence by a periodic array of dipoles. Later we shall show the effect of the charge asymmetry.

RESULTS

The dynamics of the rotational motion as described by Eqs. 1a and 1b reveals the stochastic character of the motion, including forward and backward fluctuations. Fig. 3 a shows a stochastic simulation of the trajectory, ($\theta(t)$, $z(t)$), for the helicase (three-dipole) situation showing the helical progression. The stochastic simulation method is described in Appendix A and the diffusion equation method is described in Appendix B.

The mechanical performance of the rotary motor is encapsulated in its load-velocity curve (Svoboda and Block, 1994), which is best computed from the Fokker-Planck representation of the dynamics. However, this computation is difficult if the axial and rotational motions are independent, and so we shall hereafter assume that the helicase processes such that the rotational and translational motions are coupled; that is, the protein winds along the DNA like a nut on a screw. This reduces the degrees of freedom to one, so that we can compute the rotary motion independently, then obtain the translational motion by trigonometry. The stochastic simulation in Fig. 3 a shows that the motor works without this simplification.

For this calculation we use the potential due to an "off-axis screened dipole potential" (i.e., the difference between two equal but oppositely charged exponentially screened Coulomb
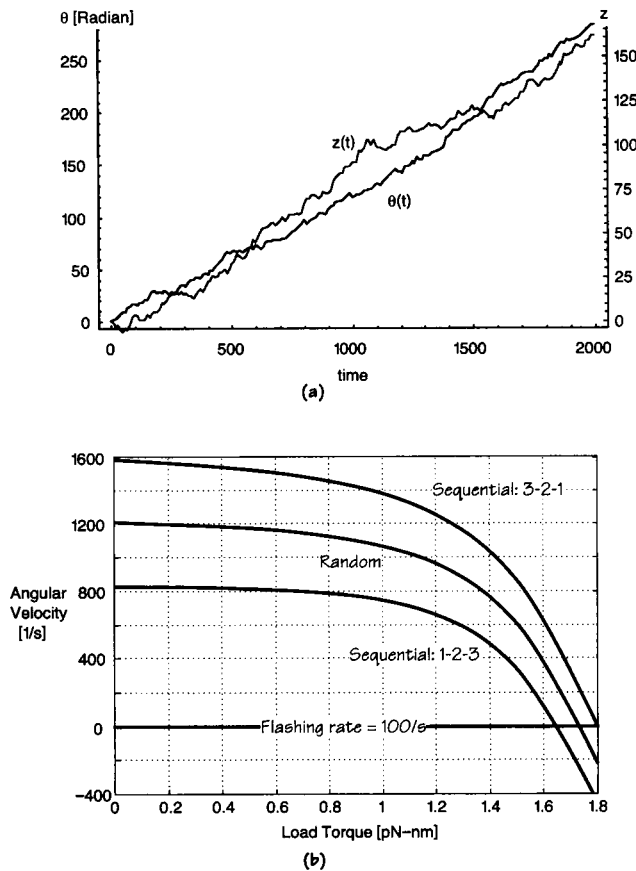
FIGURE 3 (a) Stochastic trajectory computed from Eqs. 1–3 for the helicase with three flashing dipoles interacting with two phosphates at a time. Dark line = $\theta(t)$ [radian]; gray line = $z(t)$ [nm]. (b) Load-torque/ angular velocity curve computed from the diffusion equations described in Appendix B. Some simulations were also carried out using a shooting method with the program xpp (available via WWW at http://info.pitt.edu/ ~phase/). Parameters: radius = 8 nm; well depth = 8 $k_B T$; switching rate = 100/s; inverse screening length = 50; off-axis = 0.5; D_θ = 7.5 × 10^4 nm^{TM}/s.] (ζ is estimated from the expression for the frictional drag coefficient of a cylinder of radius r spinning about its axis: $\zeta = 2\eta(\pi r^2 \ell)$, where η is the viscosity of the fluid (~0.01–0.1 poise) and ℓ, r are the length and radius, respectively. For helicase, r = 6.5 nm, ℓ = 8 nm, so that $\zeta = 6 \cdot (0.01 \text{[poise]}) \cdot (\pi \cdot 6.5^2 \cdot 8)[\text{nm}^3] \approx 6 \times 10^{-6}$ pN·nm·s. Thus the rotary diffusion coefficient $D_R = k_B T/\zeta \approx 6 \times 10^5$ s^{-1}. The volume of the portal protein is about twice that of the helicase (r $\approx$ 8 nm, h $\approx$ 10.5 nm), so its rotary diffusion coefficient is about half that of helicase. This assumes that the viscosity retarding the portal protein's rotation is equivalent to water, which is probably a low estimate.)

potentials located at $\xi = 0$, $R = r + b$, $\phi = \pi/4$) (see Fig. 7):

$$V_{dip}(x) \propto \frac{x}{b^2 + x^2} e^{-\kappa \sqrt{b^2 + x^2}} \left[\kappa + \frac{1}{\sqrt{b^2 + x^2}}\right], \quad (2a)$$

where $x = r\theta$ is the coordinate along the DNA charges (the diagonal in Fig. 2 c), κ is the inverse screening length, and b is the distance off-axis (details of the electrostatic calculations are given in the Appendix). Note that in this approximation the force acting in the translational direction is zero. The shape of V_{dip} is shown in Fig. 2 a, where the period is

the radius along the inner surface. The potential due to each dipole interacting with the array of M charges on the DNA is

$$V_{array}(x) = \sum_{m=1}^{M} V_{dip}\left(x - 2\pi \frac{m}{M} r\right). \quad (2b)$$

The time-dependent potential $V(x, t)$ acting in Eq. 1 is, at each instant of time, that due to one or another of the N phase-shifted dipoles on the inner surface of the helicase. The configuration of dipoles switches in time between the N phase-shifted configurations so that the full potential in the nth configuration can be written in terms of $V_{array}(\theta)$ according to

$$V_n = V_{array}\left(x + 2\pi r \frac{n-1}{N}\right). \quad (3)$$

The conformations realized by $V(\theta, t)$ switch among the V_n values either sequentially or randomly, as will be discussed below.

Fig. 3 b was computed using the method described in Appendix B. It shows a typical load torque-angular velocity curve for the rotary motion, comparing the performance when the hydrolysis rates at the three sites are independent, and when the hydrolysis is correlated so that the flashing proceeds sequentially. There is good evidence that, at least in kinesin, the hydrolysis rates at different sites are indeed correlated (Gilbert et al., 1995; Hackney, 1994; Peskin and Oster, 1995), so it is quite possible that the sites alternate in the rotary motors because of steric/elastic coupling. Fig. 3 shows a comparison between the mechanical performance for three "firing sequences": 1→2→3→1, 3→2→1→3, and random. Because of the asymmetry of the flashing potential, the 3→2→1 sequence outperforms the 1→2→3 sequence, with random firing intermediate between the two. (Note that in these simulations precisely a single potential is on at a time.)

Because we have assumed that the angular and axial velocities are not independent, the axial velocity along the DNA is obtained from the angular velocity times the radius by simply multiplying by the sine of the tilt angle of the dipoles; because we have chosen the dipole angle as 45°, the linear and angular motions are equal. The simulations demonstrate that the observed linear velocities required for helicase progression (~10^{-2} μm/s) are easily achievable with reasonable hydrolysis rates. The portal protein, however, requires linear velocities of ~1 μm/s, which would require hydrolysis rates beyond those observed in other ATPases. However, because the portal protein is a much larger tredecameric structure, it may have as many as 12 (or even more) hydrolysis sites. With this many flashing dipoles, the model can generate axial speeds in this range. The difficulty in simulating the portal protein is the large number of possible "firing sequences" with so many hydrolysis sites. Given the disparity in performance in the three-site helicase model, a wide range of velocities are possible for

the helicase, depending on the degree of coupling between the hydrolysis sites. Thus, given our lack of knowledge about the number and correlation of hydrolysis sites in the portal protein, we must be satisfied with demonstrating the principle of operation and forgo quantitative predictions until more kinetic and structural details are available.

Finally, measuring the statistics of the motion can give some information about the motor's underlying mechanism. Samuel and Berg (1995) measured the total time for a bacterial flagellar motor to rotate 10 revolutions under various loads. Letting T_{10} be the time to rotate 10 revolutions, a plot of log var$\langle T_{10} \rangle$ versus $\langle$velocity$\rangle = 20\pi/\langle T_{10} \rangle$ gave a slope of -2 (where $\langle \cdot \rangle$ indicates averaging over sample trajectories). That is, the relationship between the variance of the sample trajectories and the mean velocity was the same as a "Poisson stepper": at random times the motor takes a fixed size step. A constant torque motor that is free to diffuse (i.e., rotational diffusion with a constant drift angular velocity) gives a slope of -3. Therefore, they concluded that the flagellar motor had internal barriers to reverse rotation, and so was more like a Poisson stepper. On the other hand, Svoboda et al. showed that the progression of the kinesin motor was more correlated than a Poisson stepper because the trajectory variance grew more slowly than the square of the time (Svoboda et al., 1994). Fig. 3 b shows that, in the low-load regime, the velocity of the flashing field motor is almost independent of the load, and so it operates nearly as a simple Poisson stepper. At high loads, however, the velocity decreases nearly linearly with load, and reverse motion becomes more important. A plot of the log variance versus average velocity over the entire load range yields a slope of about -2.6, intermediate between the two extremes of a constant displacement and a constant torque motor. This is expected because the flashing fields impart to the rotor a constant impulse at random times, and so might be called a "Markov schtupper."

Proton-driven motors

Both the helicase and portal protein are driven by nucleotide hydrolysis. Our model posits that the elastic deformations accompanying nucleotide binding and hydrolysis are transmitted to the charge pair site. These fluctuating strains modulate the local electrostatic field acting on the phosphate charges along the DNA. There are other protein motors whose mechanism for generating torque may be similar, but which use as "fuel" not nucleotides, but ion gradients, usually protons. Examples include ATP synthase and the bacterial flagellar motor. Here we show how the flashing field model can be driven by ion gradients as well as by nucleotide hydrolysis.

Fig. 4 a shows a schematic of how such a proton gradient can produce an oscillating strain field. This strain field can be transduced into a flashing electrostatic field, which we have already shown can drive rotation. Proton channels are generally composed of one or more transmembrane α-heli-
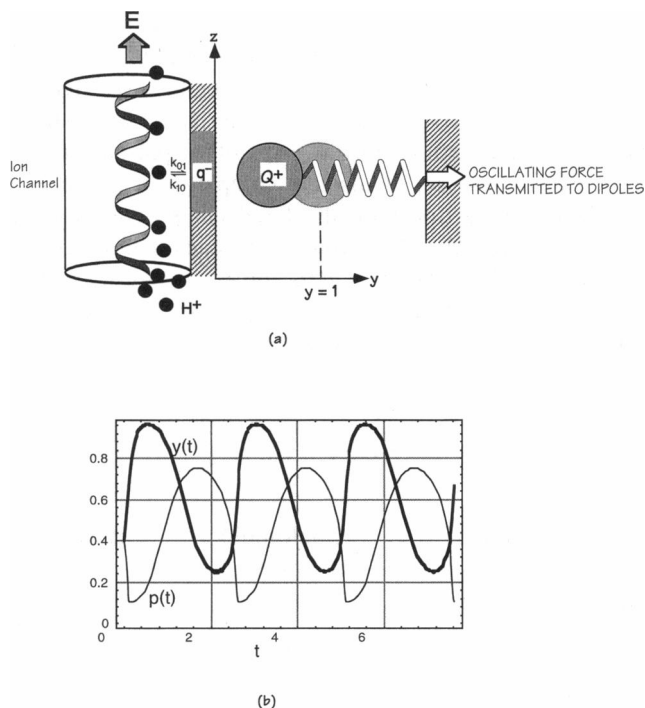

(a)

(b)

FIGURE 4   (a) Schematic of a charge-pair oscillator. Ions (e.g., protons) diffuse down their concentration gradient from $z = 0$ to $z = L$ along the hydrophillic face of an α helix. Along the way they encounter a region of negative charge, q. Their rapid association and dissociation with this region are affected by the proximity of a movable, positively charged region, depicted as the charge Q^+ on a spring. The dynamics of the system is described by Eq. 4. (b). The oscillatory dynamics computed from Eq. 4 using the illustrative parameters: $\zeta = 1$, $Q = 1$, $c_1 = 1.05$, $r = 0.1$, $k = 1$, $\tau = 20$, $k_1 = 5$, $k_{10} = 4$, $k_{20} = 300$, $k_{20} = 2$; C is normalized to unity, and the equilibrium position of Q^+ is at $y = 1$. The fluctuating strains generated by the proton flux are transmitted to the charge pair regions, which generate the flashing electrostatic field driving the rotor.

ces (e.g., Monk et al., 1994) along (or between) which the protons diffuse. We model this as a diffusion channel with periodic minima (for example, representing the fixed charges on the helical turns). Adjacent to the proton channel is a region of fixed negative charges. Nearby is an elastically tethered region of positive charge, shown schematically in Fig. 4 a as a spring (these charge regions are apparent in the structure of ATP synthase presented by Walker et al., 1994, their figure 5). Denote the movable charge region by Q and the charge region abutting the proton channel by q. Protons diffusing upward in Fig. 4 are retarded by interacting with the local field near q, which alters q's effective charge magnitude. As q decreases, the coulombic force between q and Q decreases until the movable charge, Q, is pulled away by the elastic force. As protons dissociate from the fixed charge region the coulombic attraction between the fixed and movable charges regains its strength and the movable charge, Q, once again is pulled closer to the fixed charge. To demonstrate that this qualitative picture indeed produces an oscillatory field, we describe the system mathematically as follows.

The equations describing this interaction can be formulated in terms of the ion concentration at height z, $C(z, t)$ and the coordinate of the movable charge region, $y(t)$. Because there are about five or six helical turns in traversing a bilayer, we approximate the diffusion of the protons through the channel by a set of discrete compartments, in one of which the interaction with the fixed charges takes place. Fig. 4 b shows that the proton flux causes the movable charge to oscillate. The reason for this is most easily seen by treating the protons as a single compartment adjacent to q. This yields a pair of equations similar to the van der Pol oscillator:

$$\underbrace{\zeta \frac{dy}{dt}}_{\substack{\text{Frictional force} \\ \text{on the} \\ \text{moveable charge}}} = \underbrace{-Q(c_1 - C)\frac{1 - r/y}{y^2}}_{\text{Coulombic force}} + \underbrace{k(1 - y)}_{\text{Elastic force}}$$

(4)

$$\underbrace{\frac{dC}{dt}}_{\substack{\text{Proton} \\ \text{concentration} \\ \text{at the fixed} \\ \text{charge site}}} = \frac{1}{\tau}(\underbrace{k_{10}e^{-k_1 y}(1 - C)}_{\text{Association}} - \underbrace{k_{20}e^{k_2 y}}_{\text{Dissociation}}).$$

Here τ is the time constant for proton relaxation, k is the elastic constant of the movable charge, Q, r is a "hard-core" distance limiting the motion of Q, and $(k_{10}, k_1, k_{20}, k_2)$ are rate constants governing the binding and dissociation of the protons to the fixed-charge region. In this approximation we have neglected the interaction between the protons. Increasing the dimensionality of the proton diffusion channel to many compartments, or to a continuum diffusion channel, does not change the basic dynamics: the proton flux induces reciprocating oscillations of the movable charge Q that pump the local electrostatic field; in turn, this drives the motion of the rotor as analyzed above.

Reversing the motor's direction

Whereas helicases are generally unidirectional (either $5' \rightarrow 3'$ or $3' \rightarrow 5'$), the portal protein may reverse its direction when injecting the phage DNA into the host. (Another possibility is that the free energy accumulated in packaging the DNA into the capsid is sufficient to drive injection into the host simply by entropic expansion.) The bacterial flagellar rotor spontaneously reverses its direction of rotation stochastically every few seconds. This produces the "runs" and "tumbles" characteristic of bacterial swimming (Berg and Hippel, 1985). A surprising feature of the model is that it can reverse its direction of rotation without changing the symmetry of the charge pairs. Simply altering the shape of

the potentials, for example, by changing the spacing between the charged regions, can reverse the direction of rotation.

This effect is quite counter-intuitive; it arises because of a) the asymmetry of the charge pairs (i.e., the size of the negative and positive charge regions is not identical) and b) the mismatch between the number of stator charge pairs and the number of charges with which they interact (the "vernier" effect). From Eq. 2b we can compute the average field experienced by the rotor from all of the charge pairs by integrating around the stator circumference. The asymmetry of the individual fields and the vernier effect conspire to create a net field seen by the assembly whose symmetry can switch without switching the individual charge pair symmetries. This is illustrated in Fig. 5 for the case of a stator with three charge pairs acting on a rotor where two charges are within range of their fields. For illustrative purposes we have shown the potential as a piecewise linear "wedge" whose left and right sides are of length Δl and Δr, respectively (the electrostatic field works as well but is more difficult to visualize).

Fig. 5 a is a bifurcation diagram showing how altering the shape of the potential, but not its symmetry, will reverse the direction of rotation. Therefore, to reverse the motor, the charge regions do not have to flip their polarity, but need only change their separations or angles with respect to the rotor. Fig. 5, b and c, shows this effect by illustrating the difference in symmetry experienced by a single charge and by a pair of charges rotating in the composite field of three potentials.

Because the spacing of the charges is influenced by Brownian motion, one can imagine that the operating point in Fig. 5 a could stochastically drift between clockwise and counterclockwise regions, leading to the stochastic switching behavior of the bacterial flagellar motor. We will investigate this model for the flagellar rotor more completely in another publication.

DISCUSSION

We have proposed a model for the mechanochemical operation of the rotary protein motors, DNA helicase and the portal protein. We have taken our inspiration from the recent elucidations of the structures of several rotary protein motors. In our view, the common structural features are i) the existence of multiple nucleotide hydrolysis sites located circumferentially and equally spaced in apposition to a hydrophobic channel; ii) pairs of charged regions abutting the central channel. In at least one of these structures, the F1 ATPase, the requisite structures have been identified (Abrahams et al., 1994). The model assumes that binding of nucleotide to a circumferential site induces a mechanical strain in the protein lattice that is transmitted to the charge regions. Changing the configuration of the charges with respect to one another changes the local electrostatic field

set up by the charge regions. Therefore, the negative phosphate charges that constitute the DNA backbone see a pattern of fluctuating electrostatic fields. These "flashing fields" produce a sustained electrostatic torque on the DNA. This torque does not require that the fields flash sequen-

tially; it arises because each flashing field is asymmetrical. To our knowledge, this mechanism for torque generation is novel. Fig. 6 summarizes the effects producing the rotational torque.

Surprisingly, the motor can reverse its direction in response to relatively small alterations in the shape of the potential field due to the charge pair regions. This does not require that the fields switch their polarity. Reversal results from the "vernier" effect that arises because the number of flashing fields is not the same as the number of entrained charges. This small shape modification could be controlled, for example, by phosphorylation/dephosphorylation (Goldbeter and Koshland, 1982). The bacterial flagellar rotor reverses stochastically every few seconds, and this reversal mechanism is an attractive candidate for this phenomenon.

Several authors have invoked the vernier effect in discussing the portal protein. In 1978 Hendrix pointed out that the pentagonal symmetry of the icosohedral capsid base interfaces the hexagonal symmetry of the connector (Hendrix, 1978). This led him to suggest that this symmetry mismatch might be an essential element in a rotary motor that screwed the DNA into the capsid. He reasoned that the mismatch between potential minima on the rotor and stator would produce a large number of shallow potentials that would offer little resistance to rotation. Although Hendrix did not address the mechanism of torque generation, he implied that the symmetry mismatch was somehow involved. However, later measurements showed that each base pair inserted consumed one-half ATP (Guo et al., 1987), and the 6-to-5 symmetry mismatch would consume too much ATP per revolution (Dube et al., 1993). Recent measurements also reveal that the portal protein has a 12- or 13-fold symmetry, which led Dube et al. (1993) to suggest that the rotary motor relies on the discrepancy between the tredecameric symmetry of the portal protein and the 10-fold helical symmetry of the DNA strand (Dube et al., 1993). However, they postulated that insertion was not rotary, but resulted from an axial movement. In the mechanism of force generation we have proposed, the relative motion of the rotor and stator has both axial and rotary components. The only other model we are aware of that deals with the force for packaging is the osmotic pressure model of Serwer (1988).
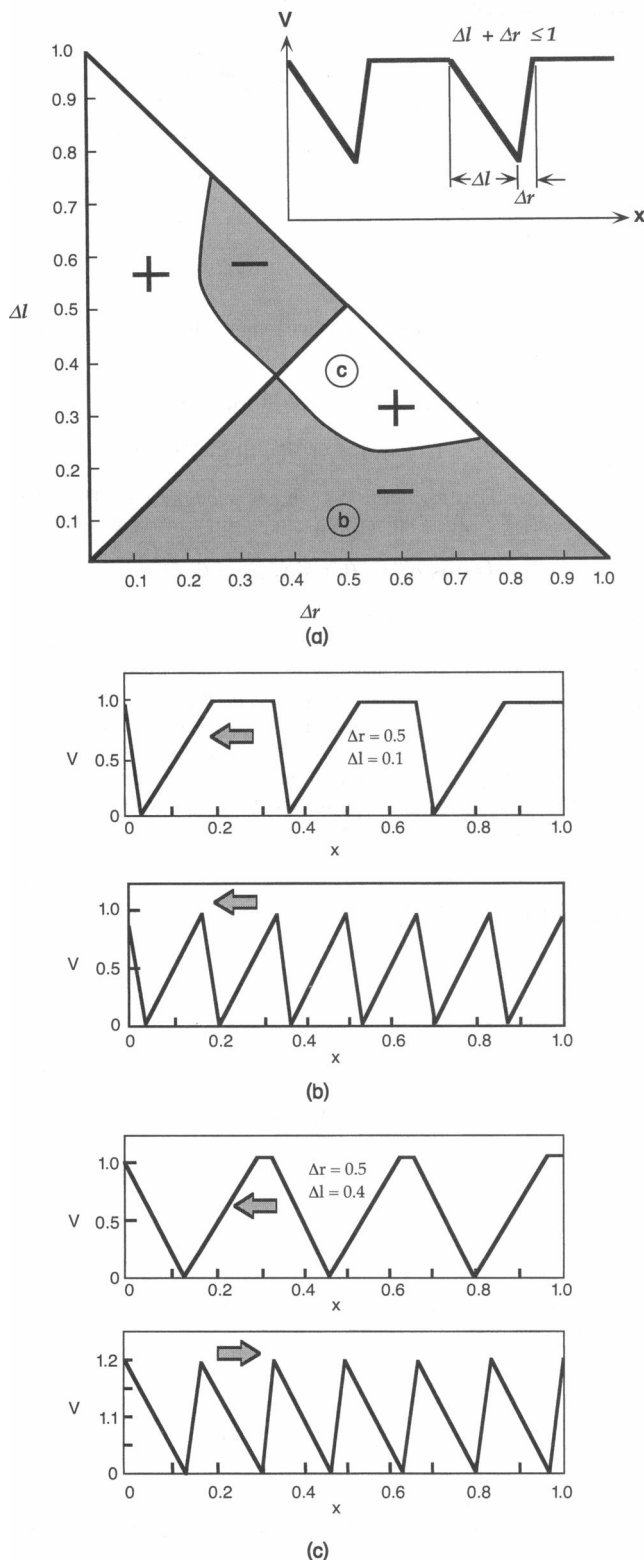
FIGURE 5   Reversing the motor. (a) The parameter plane describing the shape of the potential. In (+) regions the motor runs clockwise; in (−) regions the motor runs counterclockwise. The shape of the potential is characterized by Δl and Δr. (b and c) The shapes of the potential seen by each charge on the rotor (top) and the shapes of the potentials seen by the assembly of two charges rotating in the field of three potentials (bottom). The bottom panels were computed by inserting the potential in the top panel into Eq. 2b. In b the symmetry of the single and composite potentials are the same, and the rotor moves clockwise. In c the symmetry of the single potentials is the same as in b, but the relative steepness of the sides has changed. The rotor moves counterclockwise because the composite potential seen by both charges has symmetry opposite that seen by a single charge.

FIGURE 6   Summary of the torque-generating mechanism in the flashing field model. (*1*) Nucleotide hydrolysis, or an ion flux, produces a fluctuating strain field in the protein. (*2*) These strains alter the configuration of nearby regions of paired positive and negative charges and thereby set up a fluctuating electric field. (*3*) The asymmetry of the potentials induces a rotational torque. Brownian motion acts as a "lubricant" to ensure that the rotor does not hang up in local minima. (*4*) Because the charge pair regions are unequal, and because the number of rotor and stator charges are unequal (vernier effect), small changes in the field can cause the motor to reverse.
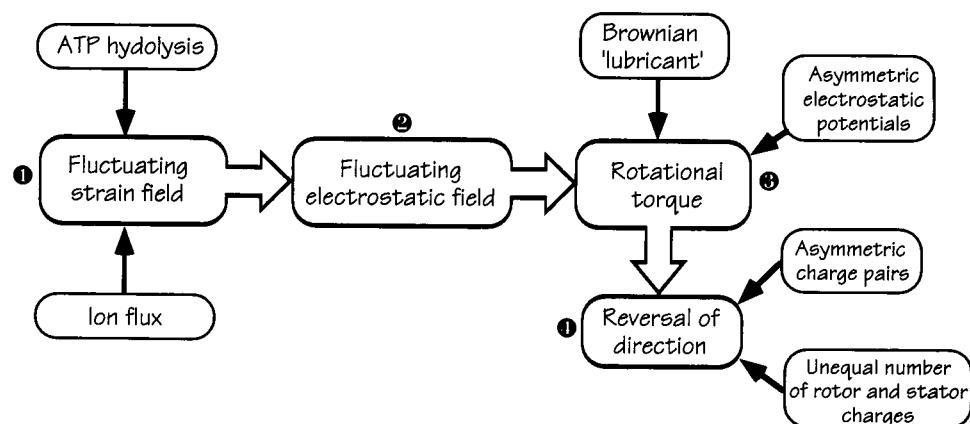
At first glance, the mechanism we have described may seem to resemble the "flashing ratchet" mechanism proposed independently by several authors (Ajdari and Prost, 1992; Astumian and Bier, 1993; Peskin et al., 1994). However, that mechanism depended on biasing the diffusion of the load by flashing an asymmetric potential, and so depended on Brownian motion in an essential way (i.e., the force vanishes as $k_B T \rightarrow 0$). The mechanism we have described here generates torque electrostatically, and the role of Brownian motion is to act as "lubrication" to jiggle the rotor out of local minima (Doering et al., 1994; Magnasco, 1993). We have also shown that the flashing field can also be driven by an ion (e.g., proton) gradient, which makes it a candidate for the bacterial flagellar motor. A similar mechanism may operate to drive the rotation of the γ subunit of ATP synthase (Abrahams et al., 1994).

How can the model be tested? The model predicts a specific form for the load-velocity relationship that appears to be different from those measured for other molecular motors (Berg and Turner, 1994; Svoboda and Block, 1994). Moreover, the statistical properties of the motor's motion are distinct from other mechanisms (Samuel and Berg, 1995; Svoboda et al., 1994). The fact that the motor is electrostatic suggests a more direct measurement: an alternating electric field imposed across the motor would interfere with torque generation when its frequency is near that of the flashing field. Although quantitative load-velocity and variance curves remain to be measured, the model makes definite predictions as to the quantities that need to measured, and provides a novel mechanism for reversible rotary motors.

APPENDIX

A. The motion of a helical array of charges driven by a flashing dipole

We consider a cylinder with radius R on which an array of dipoles centered at $z = 0$ are positioned with angle ϕ with respect to the tangent to the cylinder (see Fig. 7). Thus, $\phi = 0$ are dipoles along the radius of the cylinder with no z component. Let d be the half-distance between

the two charges; then simple trigonometry shows that the position of the charges is

$$(x^\pm, y^\pm, z^\pm) = (R \cos \xi \mp d \cos \phi \sin \xi, R \sin\xi$$

$$\pm d \cos\phi \sin \xi, \pm d \sin \phi) \tag{A1}$$

where the superscripts $\pm$ refer to the plus and minus charges. The helical array of negative charges on the DNA can be parametrized as

$$(r \cos \alpha\zeta - \theta, r \sin \alpha\zeta - \theta, \zeta) \tag{2A}$$

where r is the diameter of the DNA helix ($r < R$), α is the pitch, and the variable θ denotes the rotational component of the helix. Let the position of the charges along the helix be given by $\zeta = z + jz_0$, where z is between 0 and z_0 and j is an integer. Thus, the precise position of the helix at any given time is specified by (θ, z). Because $z = 0$ is identified with $z = z_0$, the coordinates of the helix are described by a pair of values on the torus; hence the potential felt by the charges on the DNA is a doubly periodic function. To compute this function we note that the potential felt due to a single dipole at position x_i is given by

$$V_{dip} = (\theta, z) = Q \sum_{j=-\infty}^{\infty} D^+(x_j, y_j, z_j) - D^-(x_j, y_j, z_j),$$

$$\tag{A3}$$

where

$$(x_j, y_j, z_j) \tag{A4}$$

$$= (r \cos \alpha(z + jz_0) - \theta, r \sin \alpha(z + jz_0) - \theta, z + jz_0),$$

and

$$D^\pm(x, y, z) = \frac{1}{\sqrt{(x - x^\pm)^2 + (y - y^\pm)^2 + (z - z^\pm)^2}}. \tag{A5}$$

The motion of the charges can now be computed by solving the following equations:

$$\frac{d\theta}{dt} = -\sum_{k=0}^{N-1} m_j V_\theta(\theta + j\pi/N, z) + \sigma\xi_\theta(t) \tag{A6}$$

$$\frac{dz}{dt} = -\sum_{k=0}^{N-1} m_j V_z(\theta + j\pi/N, z) + \sigma\xi_z(t), \tag{A7}$$

FIGURE 7   Geometry of the dipole locations with respect to the negative charges on the DNA backbone.

where $m_j = 1$ if the jth dipole is "on," otherwise it is zero. Here $\xi_j(t)$ are independent white noise variables. To simplify things, we assume m_j is zero except for exactly one value of j, and that the rate of transition from one state to the next is determined by r. In the simulation shown in Fig. 3, we assume no screening and take $a = 2$, $b = 8$, $c = 0.2$, $r = 20$, $\sigma = 0.5$, $N = 6$, $Q = 5$. The integration was carried out using a fixed step size of 0.01 for 200,000 steps using the program xpp.

B. Approximations to the flashing field equations

We shall model the system as a periodic sequence of charges (DNA backbone phosphates) moving through a periodic array of "off-axis-screened-dipole" potentials, each governed by Eq. 2. The phase of the underlying potential is allowed to change because of ATP-generated conformational changes moving or "turning on and off" the dipoles. The potential due to each dipole interacting with the array of M charges on the DNA is

$$V_{\text{array}} = \sum_{m=1}^{M} V_{\text{dip}}\left(x - 2\pi r \frac{m}{M}\right). \qquad (B1)$$

At each instant of time the time-dependent potential, $V(x, t)$, is due to one or another of the N phase-shifted dipoles on the inner surface of the helicase. The configuration of dipoles switches in time between the N phase-shifted configurations so that the full potential in the nth configuration is

$$V_n = V_{\text{array}}\left(x + 2\pi r \frac{n-1}{N}\right). \qquad (B2)$$

Because the number of combinations of charges and potentials is large, for simplicity in the following we consider $M = 2$ charges interacting with $N = 3$ possible dipole configurations.

Let $X(t)$ be a realization of the random process indicating the position of a phosphate along the inner radius of the helicase. The dynamics are defined by the stochastic differential equation:

$$\zeta \frac{dX}{dt} = -V'(X, t) + \sqrt{2k_B T/\zeta}\,\xi(t), \qquad (B3)$$

where ζ is the friction coefficient, $V(x, t)$ is the time-dependent potential, which at any instant is either $V_1(x)$, $V_2(x)$, or $V_3(x)$, with switching rules to be specified below, and $x(t)$ is a Gaussian white noise process satisfying

$$\langle \xi(t) \rangle = 0, \qquad \langle \xi(t)\xi(s) \rangle = \delta(t - s). \qquad (B4)$$

For notational simplicity we divide the stochastic differential equation through by ζ, identify the diffusion coefficient $D = k_B T/\zeta$, and rescale the potentials by ζ, so the equation becomes

$$\frac{dX}{dt} = -V'(X, t) + \sqrt{2D}\,\xi(t). \qquad (B5)$$

The switching dynamics are modeled as random, Markovian transitions between the different configurations. This means that the waiting time in each configuration is a Poisson distributed random variable, independent of all the other dynamics. The time scale of the switches is the inverse of the switching rate, which will be denoted α; i.e., α is the rate of jumping between subsequent configurations and α^{-1} is the average time between switches.

These stochastic dynamics are then fully described by a set of coupled Fokker-Planck equations for the evolution of the joint probabilities $P_n(x, t)$ of finding the potential in configuration n and the charge array at position x. For the case of random switching between the three configurations the equations have the form

$$\frac{\partial}{\partial t}\begin{pmatrix} P_1(x, t) \\ P_2(x, t) \\ P_3(x, t) \end{pmatrix}$$

$$(B6)$$

$$= \begin{pmatrix} F_1 - \alpha & \tfrac{1}{2}\alpha & \tfrac{1}{2}\alpha \\ \tfrac{1}{2}\alpha & F_2 - \alpha & \tfrac{1}{2}\alpha \\ \tfrac{1}{2}\alpha & \tfrac{1}{2}\alpha & F_3 - \alpha \end{pmatrix}\begin{pmatrix} P_1(x, t) \\ P_2(x, t) \\ P_3(x, t) \end{pmatrix},$$

where α is the rate of switching and the differential operator F_n is

$$F_n = \frac{\partial}{\partial x}\left\{\frac{\partial V_n}{\partial x} + D\frac{\partial}{\partial x}\right\}. \qquad (B7)$$

(In this notation, an open derivative operator like $\partial/\partial x$ operates on everything to its right.) For the case of sequential flashing in order $1 \to 2 \to 3 \to 1$

the coupled equations are

$$\frac{\partial}{\partial t}\begin{pmatrix} P_1(x,\,t) \\ P_2(x,\,t). \\ P_3(x,\,t) \end{pmatrix}$$

$$= \begin{pmatrix} F_1 - \alpha & 0 & \alpha \\ \alpha & F_2 - \alpha & 0 \\ 0 & \alpha & F_3 - \alpha \end{pmatrix} \begin{pmatrix} P_1(x,\,t) \\ P_2(x,\,t) \\ P_3(x,\,t) \end{pmatrix}, \tag{B8}$$

whereas for the reverse sequence $1\rightarrow3\rightarrow2\rightarrow1$ they are

$$\frac{\partial}{\partial t}\begin{pmatrix} P_1(x,\,t) \\ P_2(x,\,t) \\ P_3(x,\,t) \end{pmatrix}$$

$$= \begin{pmatrix} F_1 - \alpha & \alpha & 0 \\ 0 & F_2 - \alpha & \alpha \\ \alpha & 0 & F_3 - \alpha \end{pmatrix} \begin{pmatrix} P_1(x,\,t) \\ P_2(x,\,t) \\ P_3(x,\,t) \end{pmatrix}, \tag{B9}$$

For either random or sequential flashing the x-space current J is defined by the continuity equation for the marginal density $P(x,\,t) = P_1 + P_2 + P_3$ of the position variable:

$$\frac{\partial P}{\partial t} = -\frac{\partial J}{\partial x}. \tag{B10}$$

Hence the current is

$$J = -\sum_{n=1}^{3} \frac{\partial V_n}{\partial x} P_n - D\frac{\partial P}{\partial x}. \tag{B11}$$

To determine J, the full set of equations must be solved with periodic boundary conditions for $x \in [0,\,2\pi r]$ for each P_n and with the overall normalization condition

$$1 = \int_0^{2\pi r} P(x,\,t)\,dx. \tag{B12}$$

The initial distributions at $t = 0$ must be nonnegative functions satisfying the normalization condition. The average velocity of the particle is expressed in terms of the current as

$$\langle v \rangle = \int_0^{2\pi} J\,dx. \tag{B13}$$

In the steady state, $\partial P_n/\partial t = 0$, and so J approaches a constant value as the system evolves. In the steady state the average velocity is simply

$$\langle v \rangle = JL. \tag{B14}$$

This formulation is for the "no-load" situation. If an external load torque, f, is applied to the DNA, then the equivalent particle dynamics is the same

with the effective potential modified by addition of an extra term, $-fx$. Most importantly, even though the effective potential is then no longer periodic on the interval $[0,\,2\pi r]$, the coupled Fokker-Planck equations are still to be solved with periodic conditions in x.

Numerical solution is accomplished via spatial discretization of the problem wherein the continuous x variable is replaced by K discrete positions $x_k = k\Delta x$, with $k = 1, \cdots, K$ and $\Delta x = 2\pi r/KJ$. The probability densities $P_n(x,\,t)$ are replaced by probability vectors

$$\mathbf{p}_n(t) = \begin{pmatrix} p_{n,1}(t) \\ p_{n,2}(t) \\ \vdots \\ p_{n,K}(t) \end{pmatrix}, \tag{B15}$$

and the coupled Fokker-Planck equations are replaced by coupled master equations of the form (e.g., for the random switching case)

$$\frac{\partial}{\partial t}\begin{pmatrix} \mathbf{p}_1(t) \\ \mathbf{p}_2(t) \\ \mathbf{p}_3(t) \end{pmatrix}$$

$$= \begin{pmatrix} \mathbf{F}_1 - \alpha & \tfrac{1}{2}\alpha & \tfrac{1}{2}\alpha \\ \tfrac{1}{2}\alpha & \mathbf{F}_2 - \alpha & \tfrac{1}{2}\alpha \\ \tfrac{1}{2}\alpha & \tfrac{1}{2}\alpha & \mathbf{F}_3 - \alpha \end{pmatrix} \begin{pmatrix} \mathbf{p}_1(t) \\ \mathbf{p}_2(t) \\ \mathbf{p}_3(t) \end{pmatrix}, \tag{B16}$$

where the differential operators are now $K \times K$ matrices

$$\mathbf{F}_n = \begin{pmatrix} -(R_{n,1}+L_{n,1}) & L_{n,2} & 0 & \cdots & 0 & R_{n,K} \\ R_{n,1} & (-R_{n,2}+L_{n,2}) & L_{n,3} & \cdots & 0 & 0 \\ 0 & R_{n,2} & -(R_{n,3}+L_{n,3}) & \cdots & 0 & 0 \\ \cdot & \cdot & \cdot & & \cdot & \cdot \\ L_{n,1} & 0 & 0 & \cdots & R_{n,K-1} & -(R_{n,K}+L_{n,K}) \end{pmatrix}. \tag{B17}$$

The transition rates in these matrices are defined by

$$R_{n,k} = \frac{D}{\Delta x^2}\exp\left\{\frac{V_n(x_k) - V_n(x_{k+1})}{2\Delta}\right\},$$
$$L_{n,k} = \frac{D}{\Delta x^2}\exp\left\{\frac{V_n(x_k) - V_n(x_{k-1})}{2\Delta}\right\}, \tag{B18}$$

where $K + 1$ is to be interpreted as 1, and 0 is to be interpreted as K. In the absence of switching, this discretization supports a true equilibrium stationary state with vanishing currents and Boltzmann probability distributions.

The numerical solutions to these equations were carried out using MatLab on a Sun Sparcstation 20. The code is available via Internet ftp upon request.

REFERENCES

Abrahams, J., A. Leslie, R. Lutter, and J. Walker. 1994. Structure at 2.8 Å resolution of F_1-ATPase from bovine heart mitochondria. *Nature.* 370: 621–628.

Ajdari, A., and J. Prost. 1992. Mouvement induit par un potentiel périodique de basse symétrie: diélectrophorése pulsée. *C. R. Acad. Sci. Paris.* 315:1635–1639.

Astumian, R. D., and M. Bier. 1993. Fluctuation driven ratchets: molecular motors. *Phys. Rev. Lett.* 72:1766–1769.

Berg, H., and L. Turner. 1994. Torque generated by the flagellar motor of *Escherichia coli. Biophys. J.* 65:2201–2216.

Berg, O., and P. Hippel. 1985. Diffusion-controlled macromolecular interactions. *Annu. Rev. Biophys. Biophys. Chem.* 14:131–160.

Black, L. 1988. DNA packaging in dsDNA bacteriophages. *In* The Bacteriophages. R. Calendar, editor. Plenum Press, New York. 320–373.

Carazo, J. M., L. E. Donate, L. Herranz, J. P. Secilla, and J. L. Carrascosa. 1986. Three-dimensional reconstruction of the connector of bacteriophage phi 29 at 1.8 nm resolution. *J. Mol. Biol.* 192:853–867.

Casjens, S., et al. 1992. Bacteriophage P22 portal protein is part of the gauge that regulates packing density of intravirion DNA. *J. Mol. Biol.* 224:1055–1074.

Doering, C. 1990. Modeling complex systems: stochastic processes, stochastic differential equations, and Fokker-Planck equations. *In* 1990 Lectures in Complex Systems. L. Nadel and D. Stein, editors. Addison-Wesley. Redwood City, CA. 3–51.

Doering, C., W. Horsthemke, and J. Riordan. 1994. Nonequilibrium fluctuation-induced transport. *Phys. Rev. Lett.* 72:2984–2987.

Donate, L. E., and J. L. Carrascosa. 1991. Characterization of a versatile *in vitro* DNA-packaging system based on. *Virology.* 182:534–544.

Dube, P., P. Tavares, R. Lurz, and M. v. Heel. 1993. The portal protein of bacteriophage SPP1: a DNA pump with 13-fold symmetry. *EMBO J.* 12:1303–1309.

Earnshaw, W., and S. Casjens. 1980. DNA packaging by the double-stranded DNA bacteriophages. *Cell.* 21:319–31.

Egelman, H., X. Yu, R. Wild, M. Hingorani, and S. Patel. 1995. Bacteriophage T7 helicase/primase proteins form rings around single-stranded DNA that suggest a general structure for hexameric helicases. *Proc. Natl. Acad. Sci. USA.* 92:3869–73.

Gardiner, C. 1985. Handbook of Stochastic Methods. Springer-Verlag, New York.

Gilbert, S., M. Webb, M. Brune, and K. Johnson. 1995. Pathway of processive ATP hydrolysis. *Nature.* 373:671–676.

Goldbeter, A., and D. Koshland. 1982. Sensitivity amplification in biochemical systems. *Q. Rev. Biophys.* 15:555–591.

Guo, P., C. Peterson, and D. Anderson. 1987. Prohead and DNA-gp3-dependent ATPase activity of the DNA packaging protein gp16 of bacteriophage phi 29. *J. Mol. Biol.* 197:229–236.

Hackney, D. 1994. Evidence for alternating head catalysis by kinesin during microtubule-stimulated ATP hydrolysis. *Proc. Natl. Acad. Sci. USA.* 91:6865–6869.

Hendrix, R. 1978. Symmetry mismatch and DNA packaging in large bacteriophages. *Proc. Natl. Acad. Sci. USA.* 75:4779–4783.

Hingorani, M., and S. Patel. 1993. Interactions of bacteriophage T7 primase/helicase protein with single-stranded and double-stranded DNA. *Biochemistry.* 32:12478–12487.

Lohman, T. M. 1992. Escherichia coli DNA helicases: mechanisms of DNA unwinding. *Mol. Microbiol.* 6:5–14.

Magnasco, M. O. 1993. Forced thermal ratchets. *Phys. Rev. Lett.* 71: 1477–1481.

Monk, B., et al. 1994. Modeling a conformationally sensitive region of the membrane sector of the fungal plasma membrane proton pump. *J. Bioenerg. Biomembr.* 26:101–114.

Patel, S., and M. Hingorani. 1994. Nucleotide binding studies of bacteriophage T7 DNA helicase-primase protein. *In* Molecular Motors: Structure, Mechanics and Energy Transduction. Biophysical Society, Airlie, VA. 186s–189s.

Patel, S., and M. Hingorani. 1995. Nucleotide binding studies of bacteriophage T7 DNA helicase-primase protein. *Biophys. J.* 68:186s–190s.

Patel, S., M. Hingorani, and W. Ng. 1994. The k318a mutant of bacteriophage T7 dna primase-helicase protein is deficient in helicase but not primase activity and inhibits primase-helicase protein wild-type activities by heterooligomer formation. *Biochemistry.* 33:7857–7868.

Peskin, C., G. B. Ermentrout, and G. Oster. 1994. The correlation ratchet: a novel mechanism for generating directed motion by ATP hydrolysis. *In* Cell Mechanics and Cellular Engineering. V. C. Mow, F. Guilak, R. Tran-Son-Tay, and R. Hochmuth, editors. Springer-Verlag, New York. 479–489.

Peskin, C., and G. Oster. 1995. Coordinated ATPase activity explains the mechanical performance of kinesin. *Biophys. J.* 68:202s–211s.

Riskin, H. 1989. The Fokker-Planck Equation. Springer-Verlag, New York.

Samuel, A., and H. Berg. 1995. Fluctuation analysis of rotational speed of the bacterial flagellar motor. *Proc. Natl. Acad. Sci. USA.* 92:3502–3506.

Serwer, P. 1988. The source of energy for bacteriophage DNA packaging: an osmotic pump explains the data. *Biopolymers.* 27:165–169.

Svoboda, K., and S. Block. 1994. Force and velocity measured for single kinesin molecules. *Cell.* 77:773–784.

Svoboda, K., P. Mitra, and S. Block. 1994. Fluctuation analysis of motor protein movement and single enzyme kinetics. *Proc. Natl. Acad. Sci. USA.* 91:11782–11786.

Valpuesta, J., and J. Carrascosa. 1994. Structure of viral connectors and their function in bacteriophage assembly and DNA packaging. *Q. Rev. Biophys.* 27:107–155.

Valpuesta, J. M., H. Fujisawa, S. Marco, J. M. Carazo, and J. L. Carrascosa. 1992. Three-dimensional structure of T3 connector purified from overexpressing. *J. Mol. Biol.* 224:103–112.

Wong, I., and T. M. Lohman. 1992. Allosteric effects of nucleotide cofactactors on Escherichia coli Rep Helicase-DNA binding. *Science.* 256:350–356.